CrystEngComm

PAPER

View Article Online
View Journal | View Issue

Cite this: *CrystEngComm*, 2024, **26**, 4357

Anion driven tetrel bonding dictated supramolecular architectures of lead(II) with a zwitterionic form of polydentate *N*′-(piperidine-1-carbonothioyl)picolinohydrazonamide†

Ghodrat Mahmoudi, [ab] Isabel Garcia-Santos, *[c] Alfonso Castiñeiras, [c] Roi Fernández-Vazquez,[c] Masoumeh Servati Gargari,*[d] Rosa M. Gomila, [e] Antonio Frontera *[e] and Damir A. Safin *[fg]

Two novel supramolecular heteroleptic complexes $[Pb_2L_2(NO_3)_2]_n$ (**1**) and $\{[Pb_3L_3](ClO_4)_3\}_n{\cdot}3.25nH_2O$ (**2**·3.25$n$$H_2O$), obtained from *N*′-(piperidine-1-carbonothioyl)picolinohydrazonamide (**HL**) and $Pb(NO_3)_2$ or $Pb(ClO_4)_2$ in aqueous methanol are reported. A crucial role of the auxiliary ligand (NO_3^- *vs.* ClO_4^-) was revealed as a driving force for the formation of the resulting architecture of complexes, which, in turn, are dictated by the formation of tetrel bonds. Complex **1** is constructed from heteroleptic dinuclear centrosymmetric species $[Pb_2L_2(NO_3)_2]$, which, in turn, are formed from the heteroleptic mononuclear symmetry related $[PbL(NO_3)]$ units, linked through a pair of bonds formed between the metal cations and the thioamide nitrogen atoms. The metal cations form a weaker tetrel bond with the symmetry related nitrate atoms, yielding a 1D polymeric chain structure. These chains are interlinked through N–H···O hydrogen bonds, formed between the covalently coordinated nitrate oxygen atom and the NH_2 hydrogen atom, yielding a 2D supramolecular architecture. Complex **2**·3.25$n$$H_2O$ is constructed from the trinuclear species $[Pb_3L_3](ClO_4)_3$. The trinuclear cation is constructed from three $[PbL]^+$ cations interlinked through two Pb–S and two Pb–N bonds, formed with the thiocarbonyl sulfur atoms and the amide nitrogen atoms. The cations $[Pb_3L_3]^{3+}$ are interlinked through two Pb–N and two Pb–S bonds yielding a 1D supramolecular polymeric cationic chain $\{[Pb_3L_3]^{3+}\}_n$. The two metal cations corresponding to two $[PbL]^+$ units, linked through a pair of the Pb–S bonds, are additionally bridged by two oxygen atoms of one of the perchlorate anions with the formation of two Pb···O tetrel bonds. The coordination spheres of the metal cations are filled by one of the oxygen atoms of two different perchlorate anions with the formation of tetrel bonds. One of these perchlorates also forms the N–H···O hydrogen bond within the trinuclear unit $[Pb_3L_3](ClO_4)_3$. 1D supramolecular chains $\{[Pb_3L_3]^{3+}\}_n$ are interlinked through a myriad of hydrogen bonds formed by the perchlorate anions and crystallized water molecules. The tetrel bonds involving the counterions (Pb···O) have been also analysed by DFT calculations *via* a MEP surface plot and 2D maps of electron localization function (ELF), Laplacian of electron density ($\nabla^2\rho$) and reduced density gradient (RDG), confirming their noncovalent nature.

Received 11th June 2024,
Accepted 16th July 2024

DOI: 10.1039/d4ce00582a

rsc.li/crystengcomm

[a] *Department of Chemistry, Faculty of Science, University of Maragheh, P.O. Box 55136-83111, Maragheh, Iran*
[b] *Chemistry Department, Faculty of Engineering and Natural Sciences, Istinye University, Sariyer, Istanbul 34396, Turkey*
[c] *Departamento de Química Inorgánica, Facultad de Farmacia, Universidad de Santiago de Compostela, E-15782 Santiago de Compostela, Spain. E-mail: isabel.garcia@usc.es*
[d] *Western Caspian University, Baku, Azerbaijan. E-mail: masoumehservatigargari@gmail.com*
[e] *Departament de Química, Universitat de les Illes Balears, Crta de Valldemossa km 7.5, 07122 Palma de Mallorca, Baleares, Spain. E-mail: toni.frontera@uib.es*
[f] *University of Tyumen, Tyumen, 625003, Russian Federation. E-mail: damir.a.safin@gmail.com*
[g] *Scientific and Educational and Innovation Center for Chemical and Pharmaceutical Technologies, Ural Federal University named after the First President of Russia B. N. Yeltsin, Ekaterinburg, 620002, Russian Federation*

† CCDC 2360164 and 2360165. For crystallographic data in CIF or other electronic format see DOI: **https://doi.org/10.1039/d4ce00582a**

1. Introduction

In the field of inorganic chemistry, lead complexes with multidentate ligands are highly relevant because of their distinct structural and chemical characteristics.[1,2] Lead's intrinsic qualities have intrigued chemists despite its recognition as a dangerous heavy metal contaminant on a worldwide scale.[3,4] This has led to substantial research in fields such as coordination chemistry, catalysis and photochemistry.[5–13] Furthermore, the corresponding complexes are more stable and their chemical and physical properties can be precisely controlled because polydentate ligands may create strong and specific interactions with lead ions.[1–14] Therefore, comprehending the nature of these interactions and the complexes that arise is essential for expanding chemical theory as well as for developing practical applications.

Numerous noncovalent interactions are well recognized in modern synthetic chemistry, and they are an effective tool for driving crystal packing. Hydrogen bonds and π-stacking interactions are doubtlessly the most well-known and extensively applied types of noncovalent interactions.[15–21] About twenty years ago, the concept of a σ-hole was presented.[22] Subsequently, this concept gained widespread recognition as one of the key factors determining structure. According to this concept, Lewis acid atoms' σ-holes are localized electron-deficient regions that can interact with Lewis base atoms' electron-rich regions. Tetrel bonding is one of the various forms of σ-hole interactions that has received a lot of attention. An atom belonging to group 14 forms this kind of noncovalent contact as a Lewis acid.[23] The lead(II) cation (Pb^{2+}) appears to be of special interest for its potential activity to form tetrel bonding because of its large ionic radius and a rich variety of coordination numbers. Moreover, the Pb^{2+} cation's $6s^2$ lone-pair can produce either hemidirectional or holodirectional coordination.[24–27] The hemidirectional coordination environment can favor tetrel bonding and lead to the production of supramolecular architectures with extended structures. The construction and characteristics of crystal networks are largely determined by these tetrel bonding interactions. This method of approaching crystal engineering opens up new possibilities for the development of novel materials and provides profound understanding of the basic interactions that control the assembly of intricate crystal structures.

With all this in mind and in continuation of our comprehensive studies in the coordination chemistry of the supramolecular Pb^{2+} architectures as well in revealing of the role of noncovalent interactions in the formation of extended structures,[28–37] we have directed our attention on the zwitterionic form of *N*′-(piperidine-1-carbonothioyl) picolinohydrazonamide (**HL**).[38] Notably, a comprehensive search in the Cambridge Structural database (CSD) revealed only 7 known crystal structures of metal complexes derived from **HL**, namely [M(HL)Hal_2]·DMSO (M = Zn, Hal = Br;[38] M = Cd, Hal = Cl, Br, I;[39] M = Hg, Hal = Br[39]), [Cu(HL)Cl_2]·MeOH[38] and [Ni(HL)Cl]Cl,[40] and 6 crystal structures of metal complexes derived from the deprotonated form **L**, namely [ML_2] (M = Zn, Cd;[39] Ni[40]), [FeL_2]ClO_4,[38] [NiL(OAc-*O*)][40] and [Zn_2L_2(OAc-*O*,*O*′)(OAc-*O*)]·solvent.[38] Notably, all the reported metal complexes exhibit a discrete mononuclear structure, except the latter one, which is, although also being discrete, binuclear. Thus, the coordination chemistry of **HL** was poorly studied, and further research insights are required. Finally, to elucidate the nature of the Pb···O tetrel bonds observed in the self-assembled supramolecular dimers of [$Pb_2L_2(NO_3)_2$], involving the coordinated nitrate anions, DFT calculations were performed alongside MEP surface and QTAIM analyses. For [Pb_3L_3]$(ClO_4)_3$, the tetrel bonding nature of Pb···ClO_4^- contacts was also analyzed using ELF and Laplacian of the electron density 2D maps.

2. Results and discussion

A one pot reaction of $Pb(NO_3)_2$ or $Pb(ClO_4)_2$ with **HL** in aqueous methanol allowed to produce novel supramolecular heteroleptic complexes [$Pb_2L_2(NO_3)_2]_n$ (**1**) and {[Pb_3L_3]$(ClO_4)_3$}$_n$·3.25*n*H_2O (**2**·3.25*n*H_2O) (Scheme 1), which yellow plate-like and orange needle-like crystals, respectively, suitable for X-ray studies, were obtained by slow evaporation of the resulting solutions.

Structural analysis of complex **1** revealed that it crystallizes in monoclinic space group *P*2/*c* and shows the formation of a heteroleptic dinuclear centrosymmetric species [$Pb_2L_2(NO_3)_2$] (**1**) (Fig. 1). The deprotonated ligands **L** coordinate the Pb^{2+} cations through the pyridine N1 and imine N2 nitrogen atoms, and the thiocarbonyl S1 sulfur atom with bond lengths of 2.584(2), 2.395(2) and 2.7164(8) Å, respectively (Table 1). As a result, the ligand **L** forms two five-membered chelate metallocycles (Fig. 1). The dinuclear species [$Pb_2L_2(NO_3)_2$] are formed from the two [PbL(NO_3)] building units, linked through a pair of bonds formed between the metal cations and the thioamide N3′ nitrogen atoms with the bond length of 2.778(2) Å (Fig. 1, Table 1). The coordination sphere of the metal cations is filled by the oxygen atoms of the anisobidentate nitrate anion with the bond lengths of 2.593(2) and 3.062(2) Å (Fig. 1, Table 1). The metal cation exhibits a hemidirected coordination geometry that allows the formation of a weaker tetrel bond with the symmetry

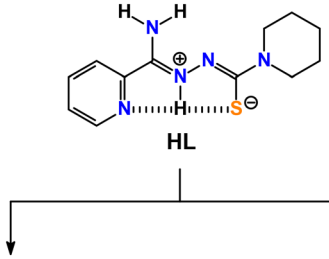

Scheme 1 Synthesis of the reported complexes.

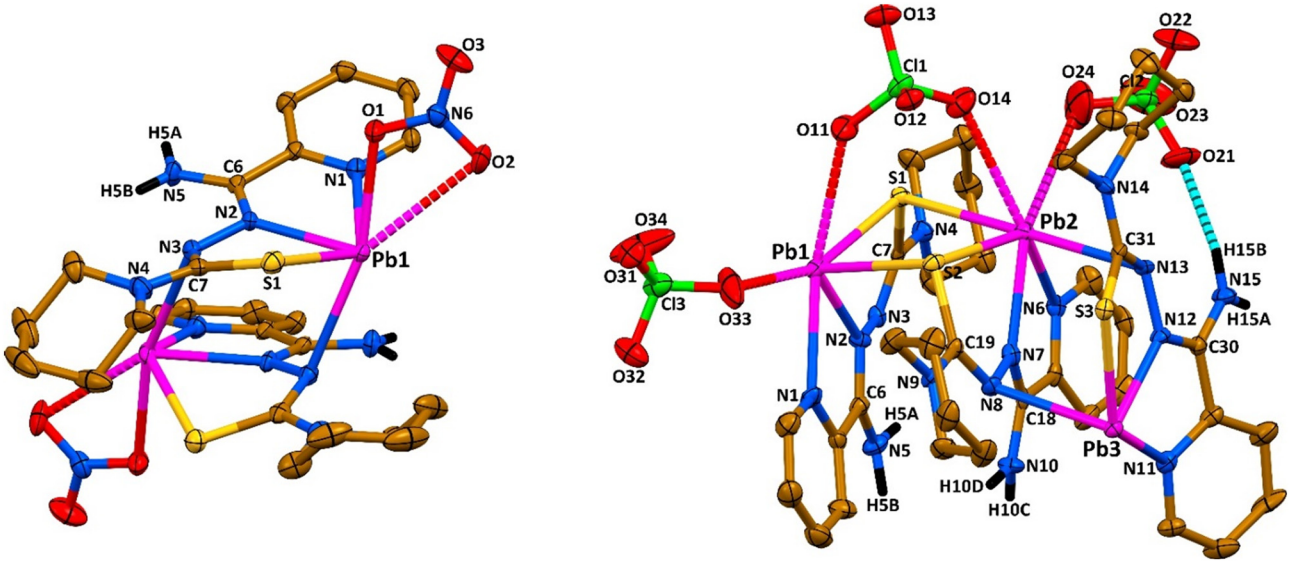

Fig. 1 Molecular structures of $[Pb_2L_2(NO_3)_2]$ (left) and $[Pb_3L_3](ClO_4)_3$ (right). CH hydrogen atoms and water molecules were omitted for clarity.

Table 1 Selected bond lengths (Å) in the crystal structures of **1** and **2**·3.25$n$$H_2O$[a]

Bond	Length	Type	Bond	Length	Type
Complex **1**			Complex **2**·3.25$n$$H_2O$		
Pb1–N1	2.584(2)	Covalent	Pb1–N1	2.585(5)	Covalent
Pb1–N2	2.395(2)	Covalent	Pb1–N2	2.425(5)	Covalent
Pb1–S1	2.7164(8)	Covalent	Pb1–S1	2.817(2)	Covalent
Pb1–N3$^{\#1}$	2.778(2)	Covalent	Pb1–S2	2.904(2)	Covalent
Pb1–O1	2.593(2)	Covalent	Pb1–N3$^{\#3}$	2.841(4)	Covalent
Pb1···O2	3.062(2)	Tetrel	Pb1···O11	3.057(5)	Tetrel
Pb1···O2$^{\#2}$	3.220(2)	Tetrel	Pb1···O33	3.317(5)	Tetrel
			Pb2–N6	2.575(5)	Covalent
			Pb2–N7	2.452(5)	Covalent
			Pb2–S2	2.800(2)	Covalent
			Pb2–S1	2.920(2)	Covalent
			Pb2–N13	2.865(5)	Covalent
			Pb2···O14	3.075(4)	Tetrel
			Pb2···O24	3.106(7)	Tetrel
			Pb3–N11	2.551(5)	Covalent
			Pb3–N12	2.380(5)	Covalent
			Pb3–S3	2.792(1)	Covalent
			Pb3–N8	2.716(5)	Covalent
			Pb3–S3$^{\#4}$	2.940(2)	Covalent
			Pb3···O22$^{\#5}$	3.125(5)	Tetrel

[a] Symmetry code: #1 1 − x, y, 1/2 − z; #2 2 − x, y, 1/2 − z; #3 1/2 − x, y, −z; #4 1/2 − x, 3/2 − y, 1/2 − z; #5 x, 1 + y, z.

related nitrate atom O2 at 3.220(2) Å (Table 1). This tetrel bonding links dimeric species $[Pb_2L_2(NO_3)_2]$ into a 1D polymeric chain structure along the a axis (Fig. 2). The polymeric chain is further strengthened by N5–H5B···O2 hydrogen bonds formed between the weakly coordinated nitrate oxygen atom and one of the NH_2 hydrogen atoms (Fig. 2, Table 2). Furthermore, the analysis of crystal packing evidences that the polymeric chains are interlinked through N5–H5A···O1 hydrogen bonds, formed between the covalently coordinated nitrate oxygen atom and the second NH_2 hydrogen atom, yielding an undulated 2D supramolecular architecture parallel to ac plane (Fig. 2, Table 2).

Complex **2**·3.25$n$$H_2O$ is built from the trinuclear species $[Pb_3L_3](ClO_4)_3$ comprising a homoleptic cation $[Pb_3L_3]^{3+}$ counterbalanced by three perchlorate anions (Fig. 1). The trinuclear cation is constructed from three $[PbL]^+$ cations interlinked through two Pb–S and two Pb–N bonds, formed with the thiocarbonyl sulfur atoms and the amide nitrogen atoms (Fig. 1). The Pb–N bonds formed with the pyridine and imine nitrogen atoms within the three $[PbL]^+$ units in the structure of $[Pb_3L_3](ClO_4)_3$ are similar to those in the structure of $[Pb_2L_2(NO_3)_2]$ (Table 1). However, the Pb–S bonds are about 0.08–0.1 Å longer in the structure of $[Pb_3L_3](ClO_4)_3$ compared to the structure of $[Pb_2L_2(NO_3)_2]$ (Table 1). This is

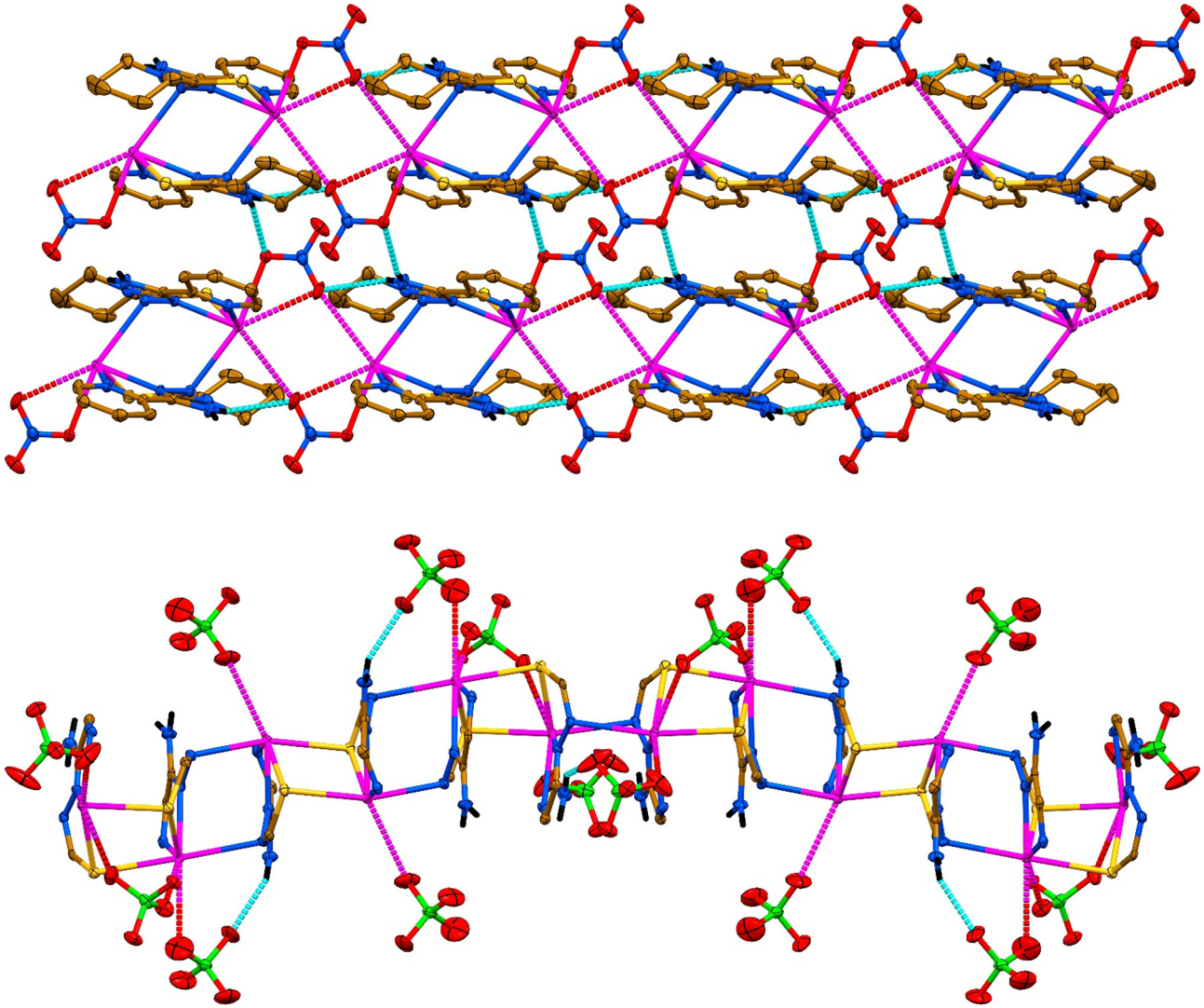

Fig. 2 (Top) A 2D supramolecular layer in the crystal structure of **1** (CH hydrogen atoms were omitted for clarity). (Bottom) A 1D supramolecular chain in the crystal structure of **2**·3.25*n*H_2O (piperidine and water molecules as well as the pyridine CH groups were omitted for clarity). Color code: H = black, C = gold, N = blue, O = red, S = yellow, Cl = green, Pb = green; Pb···O tetrel bond = red-magenta and magents dashed lines, N–H···O hydrogen bond = cyan dashed line.

explained by the formation of bridging Pb–S bonds, which are, in turn, even longer and of about 2.90–2.94 Å (Table 1), both within the structure of $[Pb_3L_3](ClO_4)_3$ and between the units $[Pb_3L_3](ClO_4)_3$ (Fig. 1 and 2). The bridging Pb–N bonds, formed with the thioamide nitrogen atoms, are 2.716(5) and 2.865(5) Å within the structure of $[Pb_3L_3](ClO_4)_3$, and 2.841(4) Å between the units $[Pb_3L_3](ClO_4)_3$ (Table 1). Thus, the homoleptic trinuclear cations $[Pb_3L_3]^{3+}$ are interlinked through two Pb–N and two Pb–S bonds yielding a 1D supramolecular polymeric cationic chain $\{[Pb_3L_3]^{3+}\}_n$ (Fig. 2).

The Pb1 and Pb2 cations corresponding to two $[PbL]^+$ units, linked through a pair of the Pb–S bonds, are further interlinked through two oxygen atoms of one of the perchlorate anions with the formation of two Pb···O tetrel bonds of about 3.06–3.08 Å (Fig. 1, Table 1). The coordination spheres of the metal cations are filled by one of the oxygen atoms of two different perchlorate anions with the formation of tetrel bonds of about 3.11–3.32 Å (Fig. 1 and 2, Table 1). One of these perchlorates also forms the N15–H15B···O21 hydrogen bond further strengthening the trinuclear unit $[Pb_3L_3](ClO_4)_3$ (Fig. 1 and 2, Table 1). Finally, 1D supramolecular polymeric cationic chains $\{[Pb_3L_3]^{3+}\}_n$ are interlinked through a myriad of hydrogen bonds formed by the perchlorate anions and crystallized water molecules (Table 2).

The first part of the theoretical study focuses on analyzing a self-assembled dimer of $[Pb_2L_2(NO_3)_2]$, extracted from the 2D supramolecular layer, which is formed by two symmetrically equivalent Pb···ONO_2 interactions (Fig. 2, magenta dashed lines). Initially, we computed the molecular electrostatic potential (MEP) surface of $[Pb_2L_2(NO_3)_2]$ to identify the nucleophilic and electrophilic regions of the complex. The MEP surface of $[Pb_2L_2(NO_3)_2]$ shows a minimum at the nitrate oxygen atoms (−55.2 kcal

Table 2 Hydrogen bond lengths (Å) and angles (°) in the crystal structures of **1** and **2**·3.25nH$_2$O[a]

D–H···A	d(D–H)	d(H···A)	d(D···A)	∠(DHA)
Complex **1**				
N5–H5A···O1$^{\#1}$	0.84(3)	2.38(3)	3.149(3)	153(3)
N5–H5B···O1$^{\#2}$	0.84(3)	2.48(3)	3.209(3)	145(3)
Complex **2**·3.25nH$_2$O				
N5–H5A···O34$^{\#3}$	0.92	2.25	3.036(7)	143
N5–H5B···O2W$^{\#4}$	0.92	2.26	3.008(6)	137
N10–H10C···O2W$^{\#4}$	0.93	2.05	2.948(6)	161
O1W–H11W···O12$^{\#5}$	0.85	2.50	2.929(6)	112
O2W–H12W···O31$^{\#6}$	0.84	2.09	2.932(6)	175
O3W–H13W···O23$^{\#4}$	0.85	2.30	3.113(7)	161
N15–H15A···O1W$^{\#4}$	0.93	1.98	2.896(7)	167
N15–H15B···O21$^{\#4}$	0.92	2.21	3.011(7)	146
O1W–H21W···O3W$^{\#4}$	0.85	1.95	2.802(6)	175
O2W–H22W···O32$^{\#3}$	0.88	2.34	3.155(6)	153
O3W–H23W···O33$^{\#5}$	0.82	2.30	3.088(8)	161

[a] Symmetry code: #1 1 − x, −y, −z; #2 −1 + x, y, z; #3 1/2 − x, y, −z; #4 x, y, z; #5 −1/2 + x, 1 − y, z; #6 −1/2 + x, 2 − y, z.

mol^{-1}) and a maximum at the NH$_2$ groups (64.4 kcal mol^{-1}) (Fig. 3). This distribution explains the formation of the N–H···O bonds (Fig. 2, Table 2), that interconnect the 1D chains propagated by Pb···O contacts. The MEP at the Pb atom is anisotropic and presents a region where the MEP is a local maximum (σ-hole), which becomes evident when a reduced scale is applied (Fig. 3). The MEP value at the σ-hole is a modest 6.3 kcal mol^{-1}.

Using quantum theory of atoms in molecules (QTAIM) analysis, we examined the centrosymmetric dimer, which is stabilized by hydrogen bonds and tetrel bonds (Fig. 3). The analysis reveals that the monomers are interconnected by six

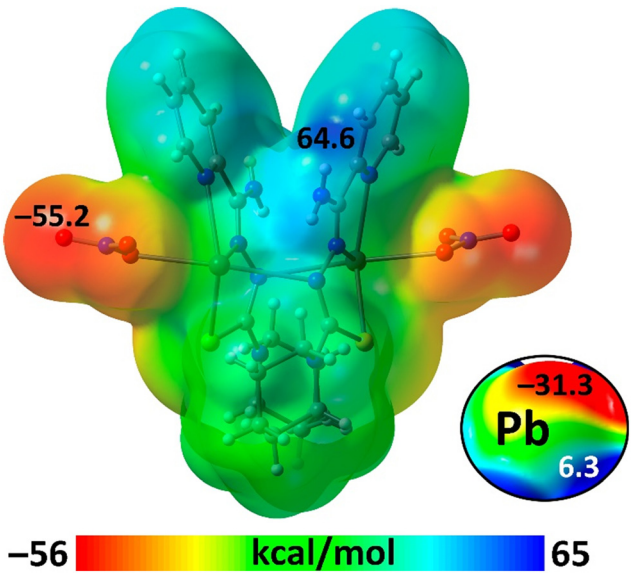

Fig. 3 The MEP surface of [Pb$_2$L$_2$(NO$_3$)$_2$] at the PBE0-D3/def2-TZVP level of theory. The MEP at the Pb atom using a reduced scale is represented in the bottom-right part of the figure.

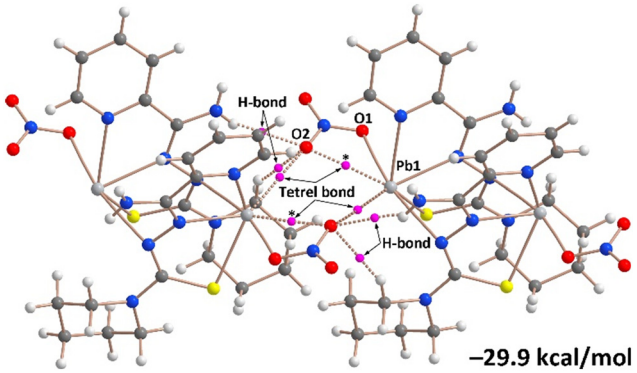

Fig. 4 QTAIM analysis of the dimer of [Pb$_2$L$_2$(NO$_3$)$_2$]. Bond critical points are shown as magenta spheres and bond paths are shown as dashed lines. The dimerization energy is indicated.

bond critical points and bond paths (Fig. 4). In addition to these intermolecular bond paths, we also show for comparison two intramolecular bond critical points (BCPs) and bond paths that characterize the Pb1···O2 contacts (Fig. 4). Therefore, each nitrate anion's O2 atom establishes four contacts: two hydrogen bonds (N–H···O and C–H···O), one intermolecular tetrel bond and one intramolecular tetrel bond. This arrangement results in a dimerization energy of −29.9 kcal mol^{-1}, highlighting the significant role of this intricate combination of interactions in the solid-state structure of [Pb$_2$L$_2$(NO$_3$)$_2$].

In the second part of the theoretical study, we further investigated the attractive and noncovalent nature of the Pb···O$_{anion}$ contacts in [Pb$_2$L$_2$(NO$_3$)$_2$] (nitrate) and [Pb$_3$L$_3$](ClO$_4$)$_3$ (perchlorate). This was achieved using a combination of 2D plots of the Laplacian of electron density ($\nabla^2\rho$) and 2D reduced density gradient (RDG) maps (Fig. 5 and 6). The $\nabla^2\rho$ 2D plot provides insights into the covalency of the interaction, while the RDG maps effectively identify regions of noncovalent interactions, making these combined maps highly useful for a comprehensive understanding of the bonding characteristics. Additionally, the sign of the second eigenvalue of the Hessian matrix of $\nabla^2\rho(\lambda_2)$ within these low RDG regions indicates the presence of attractive forces, further confirming the nature of the bond. The electron localization function (ELF) 2D map was also utilized to delineate the nucleophilic and electrophilic regions within the tetrel-bonded homodimer in [Pb$_2$L$_2$(NO$_3$)$_2$] and heterotrimer in [Pb$_3$L$_3$](ClO$_4$)$_3$.

For [Pb$_2$L$_2$(NO$_3$)$_2$], the 2D plots are detailed in Fig. 5 and supplemented by the BCP parameters compiled in Table 3, providing insights into the electronic interactions and stability characteristics of the Pb···O tetrel bonds in this dimer. The QTAIM data for the BCP that characterizes the intramolecular BCP and that of the Pb–O1 coordination bond are also included for comparison purposes (Table 3). These critical points are indicated in Fig. 5.

The 2D $\nabla^2\rho$ analysis reveals positive values (represented by solid line isocontours) between the Pb and O atoms, indicating both coordination bonds (Pb1–O1 and Pb1$^{\#2}$–O1$^{\#2}$)

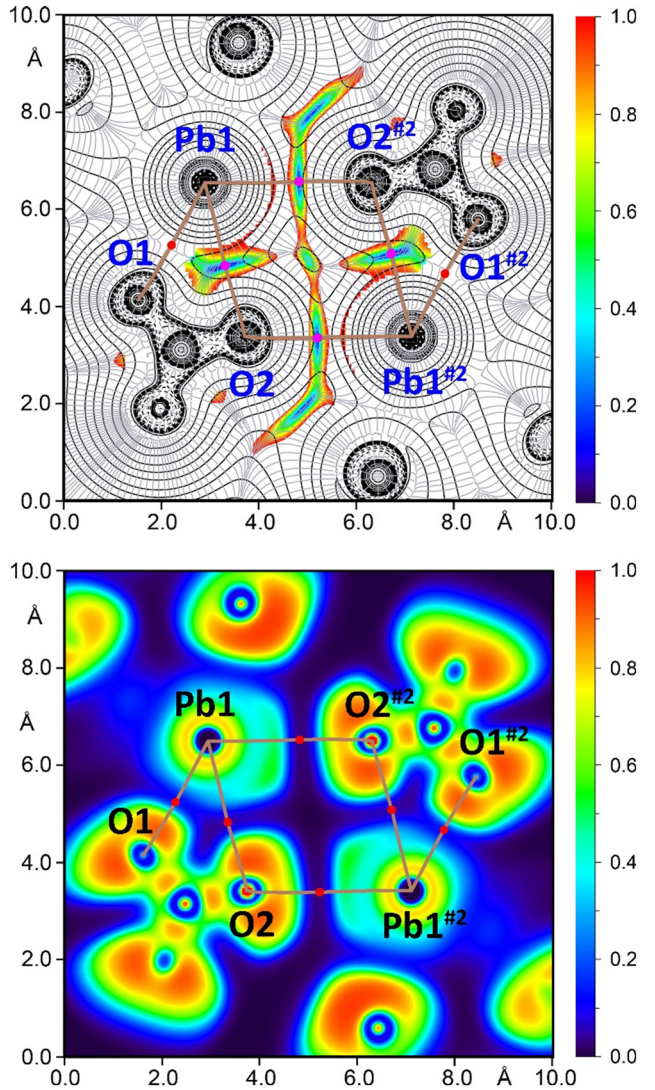

Fig. 5 A 2D plot of the Laplacian (dashed lines for negative values and solid lines for positive ones) including the gradient lines (in grey) overlapped with the 2D RDG map (top) and 2D ELF map (bottom) for $[Pb_2L_2(NO_3)_2]$. The 2D maps are represented in the mean plane defined by Pb1, O2, $Pb1^{\#2}$ and $O2^{\#2}$ atoms. The bond paths are shown as brown lines and BCPs of tetrel bonds are shown as magenta dots and those of coordination bonds as red dots. The RDG density cut-off is 0.05 a.u.

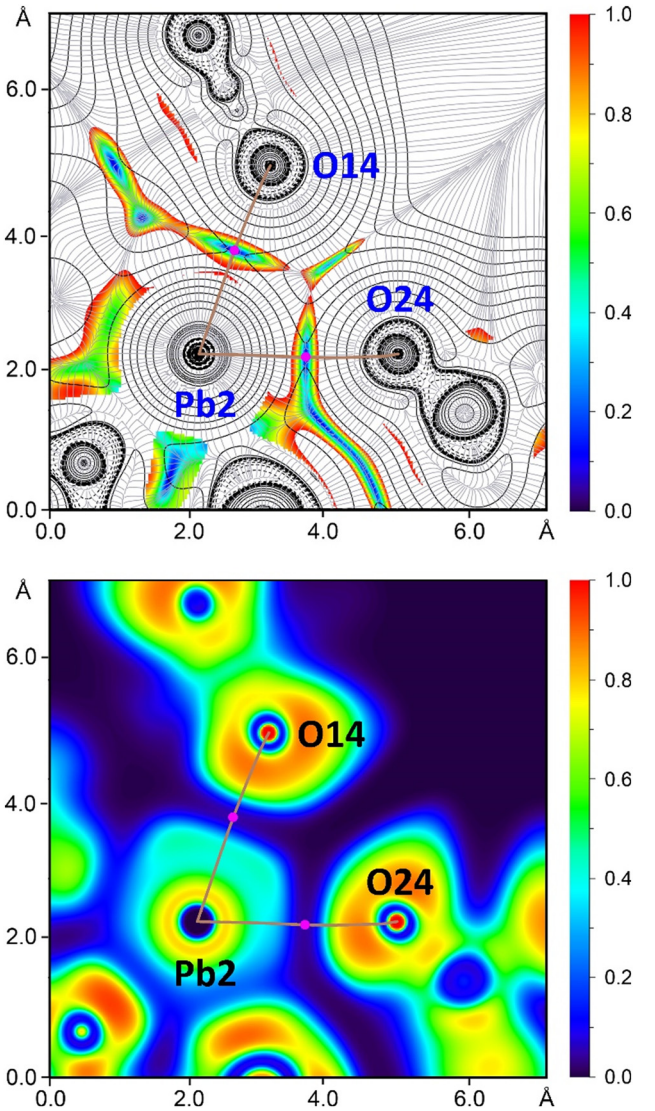

Fig. 6 A 2D plot of the Laplacian (dashed lines for negative values and solid lines for positive ones) including the gradient lines (in grey) overlapped with the 2D RDG map (top) and 2D ELF map (bottom) for $[Pb_3L_3](ClO_4)_3$. The 2D maps are represented in the mean plane defined by Pb2, O14 and O24 atoms. The bond paths are shown as brown lines and BCPs of tetrel bonds are shown as magenta dots and those of coordination bonds as red dots. The RDG density cut-off is 0.05 a.u.

and tetrel bonds (Pb1···O2 and Pb1···$O2^{\#2}$). This distinction is further emphasized by the 2D RDG map, which displays blue isocontours specifically in areas corresponding to the extended Pb···O distances (tetrel bonds), effectively differentiating them from coordination bonds. The BCPs that denote tetrel bonds are highlighted in magenta in Fig. 5, where RDG values are close to zero.

The ELF 2D map provides additional insights, highlighting the differences between Pb–O coordination bonds and Pb···O tetrel bonds. It reveals a peak in ELF at the lone pairs (LP) on the O atoms and underscores the electrophilic nature of the Pb atoms. The map also shows bluish regions (ELF = 0.13 at the BCP in red) between the Pb1 and O1 atoms involved in coordination bonds, suggesting some degree of electron localization indicative of electron sharing. In contrast, regions associated with tetrel bonds, marked by magenta BCPs in areas of minimal electron density (depicted in black), emphasize the characteristics of noncovalent interactions. This visualization confirms the weak noncovalent nature of the tetrel bonds.

The QTAIM and ELF parameters at the Pb···O BCPs of $[Pb_2L_2(NO_3)_2]$ classify the Pb1···O2 and Pb1···$O2^{\#2}$ tetrel bonds as weak (Table 3). This is evidenced by electron density (ρ) values below 0.015 a.u., small and positive values of the Laplacian of electron density ($\nabla^2\rho$), and a smaller

Table 3 QTAIM and ELF values (a.u.) for the BCPs, characterizing the tetrel bonds in $[Pb_2L_2(NO_3)_2]$ and $[Pb_3L_3](ClO_4)_3$[a]

BCP	$\rho(r)$	$G(r)$	$V(r)$	$\nabla 2\rho(r)$	ELF	λ_2
$[Pb_2L_2(NO_3)_2]$						
Pb1⋯O1	0.0367	0.0299	−0.0322	0.1106	0.1311	−0.0383
Pb1⋯O2	0.0149	0.0111	−0.0096	0.0503	0.0522	−0.0115
Pb1⋯O2$^{\#2}$	0.0049	0.0070	−0.0054	0.0341	0.0289	−0.0064
$[Pb_3L_3](ClO_4)_3$						
Pb2⋯O14	0.0127	0.0088	−0.0072	0.0414	0.0482	−0.0102
Pb2⋯O24	0.0121	0.0087	−0.0070	0.0416	0.0425	−0.0092

[a] Symmetry code: #2 2 − x, y, 1/2 − z.

absolute value of the potential energy density ($|V|$) compared to the kinetic energy density (G) at this BCP. Additionally, the negative value of the second eigenvalue of the Hessian matrix (λ_2) indicates the presence of attractive forces. Comparative data highlight the differences between the tetrel bond and the coordination bond (Table 3). Specifically, in the Pb1–O1 coordination bond, the ρ is higher than 0.03 a.u., and the value of the total energy density is negative ($H = G + V$ = −0.0023 a.u.), indicating some degree of covalency. Moreover, the values of $\nabla^2\rho(r)$, ELF and λ_2 are significantly higher for Pb2–O1, consistent with its coordination nature.

A similar analysis has been performed for $[Pb_3L_3](ClO_4)_3$, focusing on the bifurcated Pb2⋯O14 and Pb2⋯O24 contacts. They are characterized by the corresponding BCPs (Fig. 6) and bond paths linking the Pb2 atom to both perchlorate counterions. The ELF analysis clearly shows the LPs at the O atoms (red ELF regions) pointing to the σ-holes at the Pb atoms (blue ELF regions). The 2D RDG map shows low RDG regions between the anions and the Pb atoms (Fig. 6), further confirming the noncovalent nature of these contacts. The QTAIM parameters for the Pb⋯$OClO_3^-$ contacts in $[Pb_3L_3](ClO_4)_3$ are comparable to those for the Pb⋯ONO_2^- contacts in $[Pb_2L_2(NO_3)_2]$. Both sets of contacts exhibit electron density (ρ) values below 0.015 a.u., small and positive Laplacian of electron density ($\nabla^2\rho$) and total energy density ($V + G$) values at these BCPs. Additionally, the negative value of the second eigenvalue of the Hessian matrix (λ_2) in both BCPs confirms the presence of attractive forces.

Concluding remarks

In summary, we report synthesis and detailed structural analysis of two novel supramolecular heteroleptic complexes $[Pb_2L_2(NO_3)_2]_n$ (**1**) and $\{[Pb_3L_3](ClO_4)_3\}_n{\cdot}3.25nH_2O$ (**2**·3.25$n$$H_2O$). Complexes were readily obtained from the parent ligand *N*′-(piperidine-1-carbonothioyl) picolinohydrazonamide (**HL**) and $Pb(NO_3)_2$ or $Pb(ClO_4)_2$, respectively, in aqueous methanol. Complex **1** is constructed from heteroleptic dinuclear centrosymmetric species $[Pb_2L_2(NO_3)_2]$, which, in turn, are formed from the two heteroleptic mononuclear symmetry related by a crystallographic two-fold axis $[PbL(NO_3)]$ building units, linked through a pair of bonds formed between the metal cations and the thioamide nitrogen atoms. The coordination sphere of the metal cations is filled by the oxygen atoms of the anisobidentate nitrate anion. The metal cation exhibits a hemidirected coordination geometry that allows the formation of a weaker tetrel bond with the symmetry related nitrate atom. This tetrel bonding links dimeric species $[Pb_2L_2(NO_3)_2]$ into a 1D polymeric chain structure. The DFT study has evidenced that Pb⋯O tetrel bonds are stabilizing and cooperatively with other interactions contribute to the formation of the 1D polymeric chain. The polymeric chains are interlinked through N–H⋯O hydrogen bonds, formed between the covalently coordinated nitrate oxygen atom and the NH_2 hydrogen atom, yielding an undulated 2D supramolecular architecture. Complex **2**·3.25$n$$H_2O$ is built from the trinuclear species $[Pb_3L_3](ClO_4)_3$ comprising a homoleptic cation $[Pb_3L_3]^{3+}$. The trinuclear cation is constructed from three $[PbL]^+$ cations interlinked through two Pb–S and two Pb–N bonds, formed with the thiocarbonyl sulfur atoms and the amide nitrogen atoms. The homoleptic trinuclear cations $[Pb_3L_3]^{3+}$ are interlinked through two Pb–N and two Pb–S bonds yielding a 1D supramolecular polymeric cationic chain $\{[Pb_3L_3]^{3+}\}_n$. The two metal cations corresponding to two $[PbL]^+$ units, linked through a pair of the Pb–S bonds, are further interlinked through two oxygen atoms of one of the perchlorate anions with the formation of two Pb⋯O tetrel bonds. The coordination spheres of the metal cations are filled by one of the oxygen atoms of two different perchlorate anions with the formation of tetrel bonds. One of these perchlorates also forms the N–H⋯O hydrogen bond further strengthening the trinuclear unit $[Pb_3L_3](ClO_4)_3$. 1D supramolecular $\{[Pb_3L_3]^{3+}\}_n$ are interlinked through a myriad of hydrogen bonds formed by the perchlorate anions and crystallized water molecules. The noncovalent σ-hole nature of the intermolecular Pb⋯O contacts in a trimeric assembly of $[Pb_3L_3](ClO_4)_3$ has been corroborated using DFT calculations by means of 2D plots of $\nabla^2\rho$, RDG maps and ELF properties, evidencing the attractive nature of these interactions.

Complexes reported in the present work highlight developments in coordination chemistry and crystal engineering, especially as it relates to lead-based supramolecular assemblies. Because of their structural characteristics, which are mostly the result of tetrel bonding, both complexes are of potential interest for the design and

fabrication of new materials with intriguing optical or electrical characteristics.

Experimental

Materials and physical measurements

All reagents and solvents were commercially available and used as received without further purification. **HL** was synthesized according to the recently described procedure.[38]

Synthesis

A solution of $Pb(NO_3)_2$ or $Pb(ClO_4)_2$ (0.1 mmol; 33 and 41 mg, respectively) in H_2O (3 mL) was added to a solution of **HL** (0.1 mmol, 26 mg) in MeOH (30 mL). After 15 min of stirring, the solution was filtered off and was left to evaporate. After several days, crystals were obtained.

X-ray diffraction analysis

The X-ray diffraction data were collected at 100(2) K on a Bruker D8 VENTURE PHOTON III-14 diffractometer (Mo-Kα, λ = 0.71073 Å, graphite monochromator). The data were processed with APEX3 (ref. 41) and corrected for absorption using SADABS.[42] The structures were solved by direct methods using the program SHELXS-2013 (ref. 43) and refined by the full matrix least-squares technique using SHELXTL.[43] Some residuals in the difference Fourier of complex **2**·3.25*n*H_2O were assigned to water molecules (no hydrogen atoms located for O4w at occupancy 0.25). The hydrogen atoms were placed at calculated positions and constrained to ride to atoms to which they are attached, except those of the amine group of complex **1** freely refined and of the water molecules in complex **2**·3.25*n*H_2O that were located on the Fourier map.

Crystal data of 1. $C_{24}H_{32}N_{12}O_6Pb_2S_2$, M_w = 1063.11 g mol^{-1}, monoclinic, space group $P2/c$, a = 9.4676(7), b = 11.3277(11), c = 14.7065(14) Å, β = 99.769(3)°, V = 1554.3(2) Å^3, Z = 2, ρ = 2.271 g cm^{-3}, μ(Mo-Kα) = 11.013 mm^{-1}, reflections: 81 562 collected, 4748 unique, R_{int} = 0.0558, R_1(all) = 0.0185, wR_2(all) = 0.0325, S = 1.058.

Crystal data of 2·3.25*n*H_2O. $C_{36}H_{54}Cl_3N_{15}O_{15.25}Pb_3S_3$, M_w = 1765.04 g mol^{-1}, monoclinic, space group $I2/a$, a = 25.1389(10), b = 11.3401(5), c = 38.3204(19) Å, β = 102.1890(10)°, V = 10678.0(8) Å^3, Z = 8, ρ = 2.196 g cm^{-3}, μ(Mo-Kα) = 9.782 mm^{-1}, reflections: 123 133 collected, 13 253 unique, R_{int} = 0.1140, R_1(all) = 0.0352, wR_2(all) = 0.0520, S = 1.027.

Theoretical calculations

The geometries of complexes were computed at the PBE0-D3/def2-TZVP level of theory,[44–46] using the crystallographic coordinates within the Gaussian-16 program.[47] The "atoms-in-molecules" (AIM)[48] analysis of the electron density has been performed at the same level of theory using the AIMAll program.[49] The reduced density gradient (RDG)[50] and electron localization function (ELF)[51] 2D plots were computed using the Multiwfn program.[52] The QTAIM analysis was represented using the AIMAll program.[49] The Laplacian of electron density can be decomposed into the sum of contributions along the three principal axes of maximal variation, giving the three eigenvalues of the Hessian matrix (λ_1, λ_2 and λ_3). The sign of λ_2 can be utilized to distinguish bonding (attractive, $\lambda_2 < 0$) weak interactions from non-bonding ones (repulsive, $\lambda_2 > 0$).[50]

Data availability

All software packages utilized for the theoretical calculations are thoroughly described and appropriately cited in the theoretical methods section. X-ray coordinates were employed for the calculations and can be accessed from the CIF files. Crystallographic data for complexes have been deposited at the CCDC with accession numbers 2360164 and 2360165. Additionally, CIF format crystallographic data have been included as supplementary material.

Conflicts of interest

There are no conflicts to declare.

Acknowledgements

This work was supported by the grant from the Russian Science Foundation (No. 24-23-00118).

Notes and references

1 M. Kowalik, J. Masternak, K. Kazimierczuk, O. V. Khavryuchenko, B. Kupcewicz and B. Barszcz, An unusual four-nuclear Pb(II)-pyrrole-2-carboxylato polymer: The effect of the lone pair and non-covalent interactions on the supramolecular assembly and fluorescence properties, *J. Solid State Chem.*, 2019, **273**, 207–218.
2 D.-S. Liu, L.-H. Dai, F.-Q. Qiu, D.-Z. Xi, Y. Luo, N.-N. Pi and Y. Sui, Synthesis, structures and properties of lead coordination polymers based on pyridinedicarboxylate ligand, *J. Solid State Chem.*, 2021, **303**, 122540.
3 J. N. Rauch and J. M. Pacyna, Earth's global Ag, Al, Cr, Cu, Fe, Ni, Pb, and Zn cycles, *Global Biogeochem. Cycles*, 2009, **23**, 16–18.
4 S. K. Marx, S. Rashid and N. Stromsoe, Global-scale patterns in anthropogenic Pb contamination reconstructed from natural archives, *Environ. Pollut.*, 2016, **213**, 283–298.
5 W. C. D. Gruijter and T. Bokx, Luminescence of $PbCl_2$ and $PbBr_2$ single crystals. III. The blue and violet luminescence; Mechanism of energy transport, *J. Solid State Chem.*, 1973, **6**, 271–279.
6 S. K. Dutta and M. W. Perkovic, Lead as Its Own Luminescent Sensor, *Inorg. Chem.*, 2002, **41**, 6938–6940.
7 E. Irran, T. Bein and N. Stock, Inorganic–organic hybrid materials: synthesis and crystal structure determination from powder diffraction data of $Pb_2(O_3PCH_2C_6H_4CH_2PO_3)$, *J. Solid State Chem.*, 2003, **173**, 293–298.

8 Z.-M. Sun, J.-G. Mao, Y.-Q. Sun, H.-Y. Zeng and A. Clearfield, Hydrothermal synthesis, characterization and crystal structures of two new layered lead(II) diphosphonates, *New J. Chem.*, 2003, **27**, 1326–1330.

9 J.-L. Song, C. Lei, Y.-Q. Sun and J.-G. Mao, Syntheses, characterizations and crystal structures of two lead(II) phosphonate–sulfonate hybrid materials, *J. Solid State Chem.*, 2004, **177**, 2557–2564.

10 Q. Y. Liu and L. Xu, Synthesis, Crystal Structures, and Photophysical Properties of Two Novel Lead(II)–SIP Coordination Polymers (NaH_2SIP = 5-Sulfoisophthalic Acid Monosodium Salt) Containing Tetranuclear Lead(II) Units, *Eur. J. Inorg. Chem.*, 2006, **8**, 1620–1628.

11 A. M. P. Peedikakkal, H. S. Quah, S. Chia, A. S. Jalilov, A. R. Shaikh, H. A. Al-Mohsin, K. Yadava, W. Ji and J. J. Vittal, Near-White Light Emission from Lead(II) Metal–Organic Frameworks, *Inorg. Chem.*, 2018, **57**, 11341–11348.

12 J. Ni, S.-W. Wang, P.-P. Zhang, J.-J. Zhang, H. Zhao, E.-P. Tan, Z.-Y. Li, J. Chen and C. Xia, Luminescent Sensing Behaviors of a Lead Metal–Organic Framework and Its Binary/Ternary Composites: Increasing Selectivity and Sensitivity through a Multiemissive Approach, *Cryst. Growth Des.*, 2021, **21**, 207–217.

13 X.-S. Wu, R. Zhang and J.-L. Liu, *J. Solid State Chem.*, 2021, **301**, 122298.

14 D.-S. Liu, Z.-J. Qiu, X. Fu, Y.-Z. Liu, P. Ding, Y.-X. Zhu and Y. Sui, Synthesis, structures and properties of three lead coordination polymers based on ethylenediaminetetraacetate ligand, *J. Solid State Chem.*, 2019, **278**, 120879.

15 D. Sadhukhan, M. Maiti, G. Pilet, A. Bauzá, A. Frontera and S. Mitra, Hydrogen Bond, π–π, and CH–π Interactions Governing the Supramolecular Assembly of Some Hydrazone Ligands and Their MnII Complexes – Structural and Theoretical Interpretation, *Eur. J. Inorg. Chem.*, 2015, 1958–1972.

16 F. Weinhold and R. A. Klein, What is a hydrogen bond? Resonance covalency in the supramolecular domain, *Chem. Educ. Res. Pract.*, 2014, **15**, 276–285.

17 G. R. Desiraju, Reflections on the Hydrogen Bond in Crystal Engineering, *Cryst. Growth Des.*, 2011, **11**, 896–898.

18 S. J. Grabowski, Analysis of Hydrogen Bonds in Crystals, *Crystals*, 2016, **6**, 59.

19 C. A. Hunter and J. K. M. Sanders, The nature of π–π interaction, *J. Am. Chem. Soc.*, 1990, **112**, 5525–5534.

20 K. Müller-Dethlefs and P. Hobza, Noncovalent Interactions: A Challenge for Experiment and Theory, *Chem. Rev.*, 2000, **100**, 143–168.

21 C. Janiak, A critical account on π–π stacking in metal complexes with aromatic nitrogen-containing ligands, *J. Chem. Soc. Dalton Trans.*, 2000, 3885–3896.

22 T. Clark, M. Hennemann, J. S. Murray and P. Politzer, Halogen bonding: the σ-hole, *J. Mol. Model.*, 2007, **13**, 291–296.

23 Special Issue "Tetrel Bonds", **https://www.mdpi.com/journal/molecules/special_issues/Tetrel_Bonds**.

24 L. Shimoni-Livny, J. P. Glusker and C. W. Bock, Lone Pair Functionality in Divalent Lead Compounds, *Inorg. Chem.*, 1998, **37**, 1853–1867.

25 A. Bauzá, T. J. Mooibroek and A. Frontera, Tetrel Bonding Interactions, *Chem. Rec.*, 2016, **16**, 473–487.

26 A. Bauzá, S. K. Seth and A. Frontera, Tetrel bonding interactions at work: Impact on tin and lead coordination compounds, *Coord. Chem. Rev.*, 2019, **384**, 107–125.

27 I. Alkorta, J. Elguero and A. Frontera, Not Only Hydrogen Bonds: Other Noncovalent Interactions, *Crystals*, 2020, **10**, 180.

28 G. Mahmoudi, A. V. Gurbanov, S. R. Hemida, R. Corballo, M. Amini, A. Bacchi, M. P. Mitoraj, F. Sagan, M. Kukulka and D. A. Safin, Ligand-Driven Coordination Sphere-Induced Engineering of Hybride Materials Constructed from $PbCl_2$ and Bis-Pyridyl Organic Linkers for Single-Component Light-Emitting Phosphors, *Inorg. Chem.*, 2017, **56**, 9698–9709.

29 G. Mahmoudi, D. A. Safin, M. P. Mitoraj, M. Amini, M. Kubicki, T. Doert, F. Locherere and M. Fleck, Anion-driven tetrel bond-induced engineering of lead(II) architectures with N′-(1-(2-pyridyl)ethylidene)nicotinohydrazide: experimental and theoretical findings, *Inorg. Chem. Front.*, 2017, **4**, 171–182.

30 G. Mahmoudi, E. Zangrando, M. P. Mitoraj, A. V. Gurbanov, F. I. Zubkov, M. Moosavifar, I. A. Konyaeva, A. M. Kirillov and D. A. Safin, Extended lead(II) architectures engineered via tetrel bonding interactions, *New J. Chem.*, 2018, **42**, 4959–4971.

31 G. Mahmoudi, F. A. Afkhami, A. Kennedy, F. I. Zubkov, E. Zangrando, A. M. Kirillov, E. Molins, M. P. Mitoraj and D. A. Safin, Lead(II) coordination polymers driven by pyridine-hydrazine donors: from anion-guided self-assembly to structural features, *Dalton Trans.*, 2020, **49**, 11238–11248.

32 F. A. Afkhami, G. Mahmoudi, F. Qu, A. Gupta, M. Köse, E. Zangrando, F. I. Zubkov, I. Alkorta and D. A. Safin, Supramolecular lead(II) architectures engineered by tetrel bonds, *CrystEngComm*, 2020, **22**, 2389–2396.

33 G. Mahmoudi, M. Abedi, S. E. Lawrence, E. Zangrando, M. G. Babashkina, A. Klein, A. Frontera and D. A. Safin, Tetrel Bonding and Other Non-Covalent Interactions Assisted Supramolecular Aggregation in a New Pb(II) Complex of an Isonicotinohydrazide, *Molecules*, 2020, **25**, 4056.

34 I. Garcia-Santos, A. Castiñeiras, G. Mahmoudi, M. G. Babashkina, E. Zangrando, R. M. Gomila, A. Frontera and D. A. Safin, An extended supramolecular coordination compound produced from $PbCl_2$ and N′-isonicotinoylpicolinohydrazonamide, *CrystEngComm*, 2022, **24**, 368–378.

35 G. Mahmoudi, E. Zangrando, A. V. Gurbanov, B. Eftekhari-Sis, M. P. Mitoraj, F. Sagan and D. A. Safin, Tetrel bonding stabilization of a new coordination polymer constructed from lead(II) azide and 1-(pyridin-2-yl)ethylidenepicolinohydrazide, *CrystEngComm*, 2023, **25**, 5100–5108.

36 I. Garcia-Santos, T. Iglesias-Pereiro, E. Labisbal, A. Castiñeiras, B. Eftekhari-Sis, G. Mahmoudi, F. Sagan, M. P.

Mitoraj and D. A. Safin, An extended supramolecular coordination compound produced from $PbCl_2$ and N′-isonicotinoylpicolinohydrazonamide, *CrystEngComm*, 2024, **26**, 1252–1260.

37 B. Eftekhari-Sis, I. García-Santos, A. Castiñeiras, G. Mahmoudi, E. Zangrando, A. Frontera and D. A. Safin, On the pivotal role of tetrel bonding in the supramolecular architectures of Pb(II)–NCS complexes with chelating thiosemicarbazide derivatives, *CrystEngComm*, 2024, **26**, 1637–1646.

38 K. A. Ketcham, J. K. Swearingen, A. Castiñeiras, I. Garcia, E. Bermejo and D. X. West, Iron(III), cobalt(II,III), copper(II) and zinc(II) complexes of 2-pyridineforamide 3-piperidylthiosemicarbazone, *Polyhedron*, 2001, **20**, 3265–3273.

39 A. Castiñeiras, I. García, E. Bermejo, K. A. Ketcham, D. X. West and A. K. El-Sawaf, Coordination of Zn^{II}, Cd^{II}, and Hg^{II} by 2-Pyridineformamide-3-piperidyl-thiosemicarbazone, *Z. Anorg. Allg. Chem.*, 2002, **628**, 492–504.

40 K. A. Ketcham, I. Garcia, J. K. Swearingen, A. K. El-Sawaf, E. Bermejo, A. Castiñeiras and D. X. West, Spectral studies and X-ray crystal structures of three nickel(II) complexes of 2-pyridineformamide 3-piperidylthiosemicarbazone, *Polyhedron*, 2002, **21**, 859–865.

41 *APEX3 Software, v2019.11–0*, Bruker AXS Inc., Madison, Wisconsin, USA, 2019.

42 G. M. Sheldrick, *SADABS*, Bruker AXS Inc., Madison, WI-53719, USA, 1997.

43 G. M. Sheldrick, A short history of SHELX, *Acta Crystallogr., Sect. A: Found. Crystallogr.*, 2008, **64**, 112–122.

44 C. Adamo and V. Barone, Toward reliable density functional methods without adjustable parameters: The PBE0 model, *J. Chem. Phys.*, 1999, **110**, 6158–6170.

45 F. Weigend, Accurate Coulomb-fitting basis sets for H to Rn, *Phys. Chem. Chem. Phys.*, 2006, **8**, 1057–1065.

46 E. Caldeweyher, C. Bannwarth and S. Grimme, Extension of the D3 dispersion coefficient model, *J. Chem. Phys.*, 2017, **147**, 034112.

47 M. J. Frisch, G. W. Trucks, H. B. Schlegel, G. E. Scuseria, M. A. Robb, J. R. Cheeseman, G. Scalmani, V. Barone, G. A. Petersson, H. Nakatsuji, X. Li, M. Caricato, A. V. Marenich, J. Bloino, B. G. Janesko, R. Gomperts, B. Mennucci, H. P. Hratchian, J. V. Ortiz, A. F. Izmaylov, J. L. Sonnenberg, D. Williams-Young, F. Ding, F. Lipparini, F. Egidi, J. Goings, B. Peng, A. Petrone, T. Henderson, D. Ranasinghe, V. G. Zakrzewski, J. Gao, N. Rega, G. Zheng, W. Liang, M. Hada, M. Ehara, K. Toyota, R. Fukuda, J. Hasegawa, M. Ishida, T. Nakajima, Y. Honda, O. Kitao, H. Nakai, T. Vreven, K. Throssell, J. A. Montgomery Jr. , J. E. Peralta, F. Ogliaro, M. J. Bearpark, J. J. Heyd, E. N. Brothers, K. N. Kudin, V. N. Staroverov, T. A. Keith, R. Kobayashi, J. Normand, K. Raghavachari, A. P. Rendell, J. C. Burant, S. S. Iyengar, J. Tomasi, M. Cossi, J. M. Millam, M. Klene, C. Adamo, R. Cammi, J. W. Ochterski, R. L. Martin, K. Morokuma, O. Farkas, J. B. Foresman and D. J. Fox, *Gaussian 16, Revision C.01*, Gaussian, Inc., Wallingford CT, 2016.

48 R. F. W. Bader, A quantum theory of molecular structure and its applications, *Chem. Rev.*, 1991, **91**, 893–928.

49 A. Todd and T. K. Keith, *AIMAll (Version 19.10.12)*, Gristmill Software, Overland Park KS, USA, 2019, (**https://www.aim.tkgristmill.com**).

50 J. Contreras-Garcia, E. R. Johnson, S. Keinan, R. Chaudret, J.-P. Piquemal, D. N. Beratan and W. Yang, NCIPLOT: A Program for Plotting Noncovalent Interaction Regions, *J. Chem. Theory Comput.*, 2011, **7**, 625–632.

51 A. D. Becke and K. E. Edgecombe, A simple measure of electron localization in atomic and molecular systems, *J. Chem. Phys.*, 1990, **92**, 5397–5403.

52 T. Lu and F. Chen, Multiwfn: A multifunctional wavefunction analyzer, *J. Comput. Chem.*, 2012, **33**, 580–592.